Probabilistic Concepts in Intermediate-Complexity Climate Models: A Snapshot Attractor Picture

MÁTYÁS HEREIN

Institute for Theoretical Physics, Eötvös University, Budapest, Hungary

JÁNOS MÁRFY, GÁBOR DRÓTOS, AND TAMÁS TÉL

Institute for Theoretical Physics, Eötvös University, and MTA–ELTE Theoretical Physics Research Group, Budapest, Hungary

(Manuscript received 15 May 2015, in final form 23 September 2015)

ABSTRACT

A time series resulting from a single initial condition is shown to be insufficient for quantifying the internal variability in a climate model, and thus one is unable to make meaningful climate projections based on it. The authors argue that the natural distribution, obtained from an ensemble of trajectories differing solely in their initial conditions, of the snapshot attractor corresponding to a particular forcing scenario should be determined in order to quantify internal variability and to characterize any instantaneous state of the system in the future. Furthermore, as a simple measure of internal variability of any particular variable of the model, the authors suggest using its instantaneous ensemble standard deviation. These points are illustrated with the intermediate-complexity climate model Planet Simulator forced by a CO_2 scenario, with a 40-member ensemble. In particular, the leveling off of the time dependence of any ensemble average is shown to provide a much clearer indication of reaching a steady state than any property of single time series. Shifts in ensemble averages are indicative of climate changes. The dynamical character of such changes is illustrated by hysteresis-like curves obtained by plotting the ensemble average surface temperature versus the CO_2 concentration. The internal variability is found to be the most pronounced on small geographical scales. The traditionally used 30-yr temporal averages are shown to be considerably different from the corresponding ensemble averages. Finally, the North Atlantic Oscillation (NAO) index, related to the teleconnection paradigm, is also investigated. It is found that the NAO time series strongly differs in any individual realization from each other and from the ensemble average, and climatic trends can be extracted only from the latter.

1. Introduction

Climate changes are commonly described in statistical terms, in a naïve sense at least. In recent years, there is a gradually strengthening view on the internal variability of the climate system that claims that the relevant quantities are the statistics taken over an ensemble of possible realizations evolved from various initial conditions in the distant past (Hasselmann 1976; Paillard 2008; Pierrehumbert 2010; Bódai et al. 2011; Bódai and Tél 2012; Ghil 2012; Daron and Stainforth 2013, 2015). This is motivated by the sensitivity to initial conditions, a property of a complex system like Earth's climate. The relevant probability distribution is well defined and unique: independent of the particular choice of the set of initial conditions of the ensemble used in a simulation. This distribution, obtained by scanning over the initial conditions solely, naturally captures the internal variability of the dynamics, unlike, for example, perturbed physics ensembles (Stainforth et al. 2005). As pointed out in Drótos et al. (2015), to obtain this relevant probability distribution one has to consider any specific ensemble after a finite convergence time has passed from the initialization. This also means that, in the terminology of IPCC (2013), uninitialized climate projections should be considered in order to characterize climate changes.

The mathematical concept that provides the appropriate probability distribution is that of snapshot

Corresponding author address: Gábor Drótos, Institute for Theoretical Physics, Eötvös University, Pázmány Péter sétány 1/A, H-1117 Budapest, Hungary.
E-mail: drotos@general.elte.hu

DOI: 10.1175/JCLI-D-15-0353.1

(Romeiras et al. 1990; Drótos et al. 2015) or pullback attractors (Arnold 1998; Ghil et al. 2008; Chekroun et al. 2011), originally arising in the study of dissipative nonautonomous systems (Arnold 1998). Loosely speaking, a snapshot attractor, as introduced by Romeiras et al. (1990), is an object belonging to a given time instant that is traced out by an ensemble of trajectories randomly initialized in the remote past, while all of them are governed by the same equation of motion. A pullback attractor is a similar object associated with the entire real time axis ($-\infty < t < \infty$). A snapshot attractor can be considered as a time slice (corresponding to a given time instant) of a pullback attractor.

Qualitatively speaking, a snapshot or pullback attractor is nothing but the attractor of the dynamical system, a unique object of the phase space, to which trajectories converge within a basin of attraction. As a consequence of the dissipative nature of the dynamics, the initial conditions of a trajectory are ''forgotten''; that is, with increasing time, the evolution of the particular trajectory becomes independent of its initial position within the basin of attraction. The attractor characterizes the long-term behavior of initially different trajectories. This implies that a trajectory, as it evolves in time, cannot leave the attractor after reaching it. The attractor itself, however, may depend on time, and this is uniquely determined by the forcing scenario of the dynamical system. The adjective *snapshot* or *pullback* is used when the forcing depends arbitrarily on time. This is intended to express the contrast with ''usual'' attractors belonging to the special case of temporally constant or periodic forcings. This distinction in the terminology is justified by the fact that the theory of usual attractors relies on the presence of (perhaps an infinite number of unstable) periodic orbits (see, e.g., Ott 1993), but no such orbits can be present in the general case, implying that usual methods break down. An important feature of the usual case is that this attractor can be obtained either by following a single trajectory for a very long time or by monitoring an ensemble of trajectories for a shorter time (so that the dynamics is called ergodic, at least when one attractor is present in the phase space). Snapshot or pullback attractors corresponding to aperiodic forcings emerge, however, in the ensemble picture only, while a traditional single-trajectory plot in the same problem would be unable to characterize any instantaneous state of the system. In fact, snapshot or pullback attractors can be considered as the generalization of usual attractors for the case of arbitrarily time-dependent forcing.

The mathematical definition of a snapshot or pullback attractor (see Kloeden and Rasmussen 2011; Carvalho et al. 2013) relies on the limit of infinitely remote initial conditions. Such initiation is, however, hardly meaningful in large-scale climate simulations. Here, following Drótos et al. (2015), we propose a more practical approach. In a dissipative dynamical system a trajectory may be expected to lose its dependence on initial conditions according to an approximately exponential law in time, characterized by a relaxation time τ over which the value of an exponential function decreases by a factor of e. (This can be so even in high-degree-of-freedom dynamical systems as we shall illustrate within an intermediate-complexity GCM.) Therefore, ensembles of trajectories with different initial distributions can be considered to be independent of the particular initial distributions a few times τ (which we shall call the convergence time t_c) after the instant of their initiation. The single set emerging this way is thus defined with an exponential accuracy, and, according to its attracting nature, it is nothing but the snapshot attractor. We then conclude that the snapshot attractor and its probability distribution is practically well defined after t_c has passed since the initiation. The sketched picture implies that the ensemble should be initialized a time t_c before the beginning of the meaningful observations (instead of the infinitely remote past requested in the mathematical literature).

As also argued in Drótos et al. (2015), the use of snapshot attractors is most natural (or, even more, unavoidable) when dealing with climate changes induced by smoothly shifting parameters. In this situation the snapshot framework is the only one in which a probability distribution, the well-defined instantaneous distribution (in mathematical terms, the natural measure) on the snapshot attractor, can be associated with the dynamics. This distribution is time dependent, just like any climate-related average taken with respect to this distribution. More generally, climate changes can be considered as the change of snapshot attractors and their natural distributions in time [as pointed out first in Bódai and Tél (2012)].

This approach to climate can be contrasted with the traditional one (IPCC 2013; Bye et al. 2011), based on 30-yr (or multidecadal) temporal averages originating in observational data and thus being taken along a *single* realization in our language. These temporal averages are mostly considered as reference values, characterizing a climatic state. Temporal averages are also used for evaluating projections for the future [in particular, IPCC (2013, annex I) uses 20-yr windows]. For consistency, we shall keep a 30-yr window width when evaluating single-realization temporal averages in our model at any time. For simplicity, we do not split the interval of investigation into disjoint 30-yr parts but let them overlap continuously.

The basic conceptual difference between the snapshot and the traditional approach is that the data derived

from the traditional one depend on the particular realization and thus cannot reflect the behavior of all possible realizations. We believe that restricting the observations to a particular, unrepresentative realization is not useful if one intends to understand how the climate system can behave. Instead, a complete probability distribution should be considered, as captured by the snapshot attractor approach. In addition, the traditional approach involves an arbitrary choice of a finite-length time window, while the snapshot picture is inherently instantaneous. This is important because a time interval of finite length may smooth trends that are present in the time evolution of the probability distribution appropriately describing the climate system. These trends are naturally included without any bias or distortion by the instantaneous snapshot attractor approach.

The evaluation of different snapshot-type statistics might thus be appropriate in any large-scale climate model. In this direction the first steps were, perhaps, made by Goosse et al. (2005) and Deser et al. (2012a,b) when estimating the internal variability from ensemble runs, although without taking care if they waited long enough to assure their ensemble of initial conditions to converge to a dynamical attractor. Our aim here is to carry out a consistent snapshot approach within the framework of an intermediate-complexity climate model, the Planet Simulator (Fraedrich et al. 2005a), where we ensure that the convergence to an attractor took place (which requires in this example a time lag of at most a few hundred years after initialization).

Within the snapshot attractor picture, novel features of our work are the utilization of a high-degree-of-freedom model system and the consideration of a deterministic and piecewise linearly changing forcing via the CO_2 content. In our scenario, a doubling of the CO_2 takes place over 100 years, then the concentration suddenly turns to be constant, and after a plateau of 350 years, the concentration decays linearly, again within a 100-yr interval, back to the original value. We find that not even the ensemble averages follow this forcing quasi-statically (i.e., there is a nonlinear deviation from the CO_2 trend). As a consequence, a *dynamical hysteresis* (Fraedrich 2012) can be observed on the plane spanned by the CO_2 content and the ensemble average. Furthermore, the internal variability is found to be the strongest on small geographical scales where any individual time series considerably deviates from the corresponding ensemble average. The traditionally used 30-yr temporal averages are also shown to strongly differ from the ensemble averages. We also consider teleconnections (i.e., correlation between quantities defined by observing remote locations). The example of the North Atlantic Oscillation (NAO) index illustrates that even this time series strongly differs in any individual realization from the ensemble average, and climatic trends can be extracted only from the latter. Properties like the dependence of internal variability on the geographical scale, or like the limited possibility of extracting local climatic trends from individual realizations of climatic variables, cannot be obtained from low-order models, only from high-degree-of-freedom systems, such as the Planet Simulator.[1]

The paper is organized as follows. In section 2 we briefly introduce the Planet Simulator model and our particular setup. In section 3 we present our primary results regarding snapshot attractors on the example of small-scale variables. Individual time series exhibit strong fluctuations, and the system has a definitely nontrivial response on the applied CO_2 scenario. The time after which an ensemble reaches the snapshot attractor turns out to be about 150 years in our case. Section 4 contains our findings concerning a dynamical hysteresis between the average surface temperature and the CO_2 content, in which strong dependence on the spatial scale can also be observed. A comparison between the traditional approach of using 30-yr temporal averages (over a single realization) and the novel snapshot picture using ensemble averages is given in section 5, with special emphasis on relaxation times. Section 6 is devoted to the investigation of NAO time series in a changing climate and can be considered as a first application of the snapshot technique to teleconnection analysis. The last section contains our final remarks.

2. The Planet Simulator and the model setup

The climate model used is the Planet Simulator (PlaSim), version 16 (Fraedrich et al. 2005a; Fraedrich 2012), an open-source (freely available under http://edilbert.github.io/PLASIM/) general circulation model of intermediate complexity, developed at the University of Hamburg. The dynamical core of PlaSim is based on the Portable University Model of the Atmosphere (PUMA; Fraedrich et al. 1998, 2005b).

The atmospheric dynamics is described by the primitive equations, which represent the conservation of momentum and mass, the first law of thermodynamics, and the hydrostatic approximation. The equations are formulated for vorticity, divergence, the logarithm of

[1] We emphasize that this study is intended not to make any accurate projections for Earth climate but rather to illustrate its fundamental variability.

the surface pressure, and temperature. They are solved via the spectral method applied to the sphere (Orszag 1970). The unresolved processes are parameterized; parameterizations consist of interactive clouds (Stephens et al. 1984) and of shortwave (Lacis and Hansen 1974) and longwave (Sasamori 1968) radiation. Boundary layer fluxes of latent and sensible heat, as well as vertical and horizontal diffusion, are taken into account. Water vapor transport is treated with special care via moist air convection and parameterized large-scale precipitation. The annual cycle of insolation is built in. Greenhouse gases (viz. water vapor, carbon dioxide, and ozone) are also parameterized, and their effect is included in the calculation of the transmissivities (Sasamori 1968). The global concentration of CO_2 directly influences the radiative transfer of the atmosphere because there are no sinks or sources (as there is no absorption of CO_2 into water and the standard configuration does not treat the biosphere). Instead, the CO_2 concentration can be externally controlled even as a time-dependent forcing. A detailed description of PlaSim can be found in Lunkeit et al. (2011).

PlaSim has been used in previous studies—for example, to investigate the global energy and entropy budget (Fraedrich and Lunkeit 2008; Lucarini et al. 2010), to examine the response function formalism for climate changes (Ragone et al. 2015), and to analyze the late Permian climate (Roscher et al. 2011). It should be noted that PlaSim is designed to contain the fundamental physics of the climate system without all the details of cutting-edge GCMs. It is thus ideally suited for conceptual investigations like ours.[2]

In the present study we use the default PlaSim setup: the atmosphere is coupled to a nonmoving mixed layer ocean (Stephens et al. 2005) without any hydrodynamical activity. Nonetheless, horizontal heat fluxes, obtained from general circulation data, are incorporated (thus, e.g., oceanic currents like the Gulf Stream are thermally specified). The oceanic compartment interacts with the atmosphere only via heat and moisture exchange, and it has a thermodynamic sea ice module as well. The atmospheric dynamics is treated in 10 vertical levels in σ coordinates ($\sigma = p/p_s$, where p and p_s denote pressure and surface pressure, respectively). The resolution of the model is T21 in the horizontal direction [i.e., spherical harmonics up to degree $l = 21$ are treated, which can also be represented by a 64×32 Gaussian grid (Washington and Parkinson 2005) on the surface of the Earth]. Default PlaSim parameters are used: a year consists of 365 days (366 for leap years), the time step is 45 min, and the solar constant is 1365 W m^{-2}. The only exception to the default setup is the mixed layer depth that we choose to be 200 m in order to be closer to oceanographic data and to achieve more realistic atmospheric relaxation times than with the standard PlaSim setting of 50 m.

PlaSim's mixed layer ocean corresponds, of course, to neglecting the internal variability originating in the oceanic large-scale hydrodynamics (Dijkstra and Ghil 2005). This choice can be justified when concentrating on time intervals much shorter than the characteristic time scale of this slow internal variability, which is estimated to be on the order of 1000 years. This is the case in our particular investigation. A more precise study of the climate system, which incorporates ocean–atmosphere interactions in detail [such as in Feliks and Ghil (2011) for the NAO], would require an increase of the resolution and a more refined model than PlaSim. This is, however, beyond the scope of our conceptual investigation because our PlaSim setup proves to be sufficient for demonstrating the applicability of the snapshot view to high-degree-of-freedom models.

Here we concentrate on the impact of a CO_2 forcing on the surface temperature and other climatic variables on a global scale, large scale, and small scale. The latter two are chosen to correspond to Europe (or to the scale of the Rossby wavelength, in the language of geophysical fluid dynamics) and to a single grid point representing the smallest scale on which results can be obtained from the model. In particular, surface temperature values for these two scales are obtained by applying a mask over the globe that keeps geographical locations only belonging to Europe and to a grid point within continental Europe, respectively, and then taking the surface mean (if applicable) of the temperature values that are kept by the mask. For the global scale, no mask is applied.[3]

We investigate the often-used scenario of CO_2 doubling, augmented after some time with a symmetric decrease of the CO_2 concentration $c(t)$ back to the original level. This reference level is 360 ppm, which is doubled over a ramp of 100 years at a constant rate, and after a 350-yr plateau the concentration decreases back to its initial value, linearly, over 100 years again:

[2] Note again that our investigation, accordingly, does not aim to produce any precise climate projections.

[3] The grid indices that are kept by the masks are the following: Europe (large scale): 63, 64, 1, . . . , 7 (from 11°W to 33°E) in longitude and 4, . . . , 10 (from 35° to 69°N) in latitude. Single grid point (small scale): 4 (17°E) in longitude and 8 (47°N) in latitude. The surface means are calculated as area-weighted sums over the grid points divided by the spherical surface area.

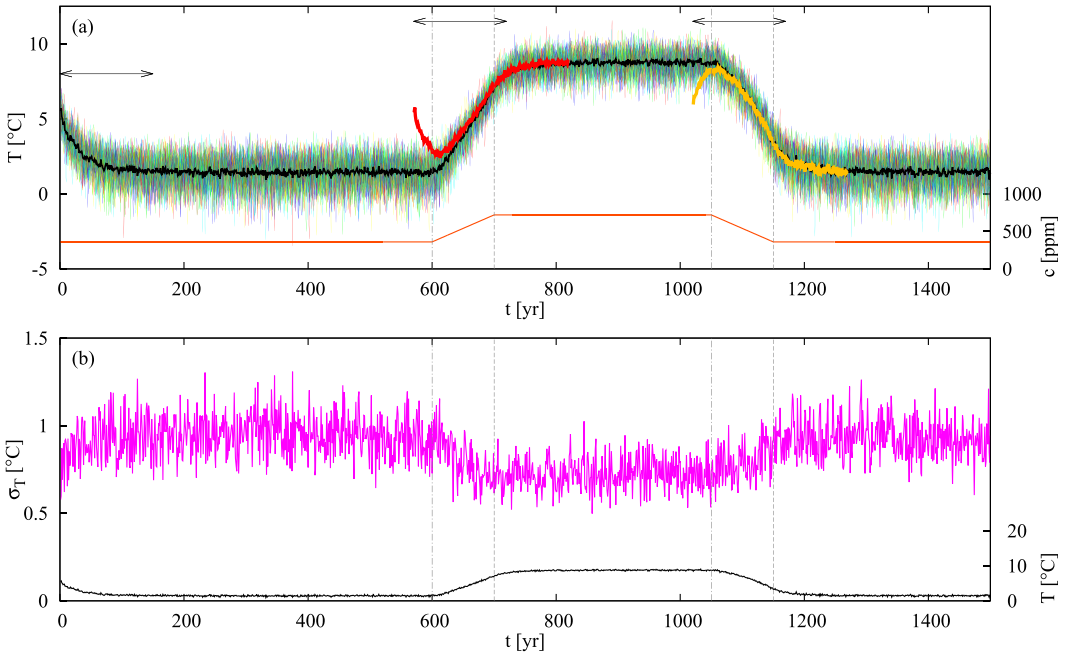

FIG. 1. Ensemble results for the small scale. (a) Annual mean surface temperature T as a function of time. Results for individual ensemble members initialized at $t_0 = 0$ are plotted in different colors, and the ensemble average of these values is marked as a black line. To demonstrate the attracting property, the average over two additional ensembles, initialized at $t_0' = 570$ and $t_0'' = 1020$ yr, are also shown in red and light orange, respectively. The convergence time $t_c \approx 150$ yr is marked by black horizontal arrows. The forcing $c(t)$ is also included in dark orange. The vertical dot–dashed (dashed) lines in gray mark the beginning (end) of the ramps in $c(t)$. (b) The ensemble standard deviation σ_T (magenta) of T over the same time period. For comparison, the ensemble average of T is shown in black [as in (a), but on a different vertical scale].

$$c(t) = \begin{cases} 360 & \text{for} \quad 0 < t < 600 \quad \text{and for} \quad 1150 < t < 1500, \\ 360 + 3.6(t - 600) & \text{for} \quad 600 < t < 700, \\ 720 & \text{for} \quad 700 < t < 1050, \\ 720 - 3.6(t - 1050) & \text{for} \quad 1050 < t < 1150. \end{cases} \tag{1}$$

(Units are year and ppm for time and concentration, respectively.) The length of the CO_2 plateaus is chosen such that a convergence to a steady climate (to be discussed in section 3) can take place much before the end of the plateaus. The slope in the interval between years 600 and 700 corresponds to a "standard scenario," but, as a novelty, we also consider the decreasing counterpart of the latter.

3. Primary results

To have a feeling of how snapshot attractors appear in intermediate-complexity climate models, we run PlaSim with the built-in initial temperature profiles and the built-in hydrostatic atmosphere initially at rest, but we slightly perturb the initial surface pressure field in $N = 40$ different replicas. The difference among these pressure fields is a random perturbation of maximum 10 hPa (as provided by the "kick" routine; see Lunkeit et al. 2011). An ensemble is created this way, and each member's time evolution is monitored from the time instant $t_0 = 0$ of the initiation over the full observational period of 1500 years with the CO_2 forcing scenario described by Eq. (1). All the atmospheric parameters, including the solar constant, are as in the default PlaSim setup. The fact that the initial conditions might appear to be unrealistic, in particular in several copies, is in fact favorable because one can be sure this way that any initial condition results in a meteorologically accessible circulation pattern as a result of the existence of an attractor. Furthermore, the use of 40 different realizations enables us to explore the internal variability on the attractor.

For a first impression, we show in Fig. 1a the annual mean surface temperature T for all the ensemble members (plotted in different colors) on the small scale. The ensemble average of these values is marked as a black line. A striking observation is the strong deviation of the individual ensemble members from the average; the individual colored lines "oscillate" around the black one, and fluctuations of the order of 2°C appear to be quite typical.

Another interesting feature is that after year 150 all the individual curves and also their ensemble average appear to follow the trend of the CO_2 scenario (included as a dark orange line), although qualitative differences are also present even in the ensemble average: the breakpoints of the CO_2 scenario are smoothed out, most pronouncedly about years 700 and 1150.

Before analyzing the temperature response in more detail, it is worth focusing on the initial period of the first $t_c = 150$ yr (which turns out to be the convergence time). In the full period of the first 600 years there is no change in the CO_2 forcing. The temperature values, however, follow a decreasing trend in the first 150 years. This is due to the fact that the initial wind and pressure fields were rather far away from those of a steady climate corresponding to a constant CO_2 concentration of 360 ppm. The temperature of the first year happens to lie in the range of 4–6°C for the different members, with an average about 5°C, while the steady climate temperature corresponds to approximately 2°C. What we see in the first $t_c = 150$ yr is a transient relaxation of the initial ensemble to a state with time-independent averages (i.e., to the steady climate).

In the language of dynamical systems' theory the initial points in the high-dimensional phase space converge in t_c to an attractor. This can be considered to be an example of a snapshot attractor (as described in the introduction), but actually it is simpler: in the absence of any time-dependent driving (when considering annual or seasonal means) this is a usual attractor. The deviation of the individual curves from the average indicates that the attractor is chaotic (individual trajectories, even if they come close to each other in an instant, strongly deviate afterward). The scatter from the average is a measure of the internal variability in the particular, steady climatic state. The probability distribution underlying the instantaneous (i.e., corresponding to a particular year) annual temperature values of the ensemble reflects the natural distribution on the attractor. Because of this probabilistic aspect of the instantaneous values, we shall refer to the individual time series in the PlaSim model as individual realizations. The climatic state is steady if the natural distribution is time independent (implying the ensemble averages are constant). In our annual mean temperature representation this means that the graph of the ensemble average traces out a plateau.[4] In the first 600 years this occurs after year 150, but we find temperature plateaus in the intervals approximately [800, 1050] and [1300, 1500] yr, too.

The really interesting region, also from the point of view of attractors, is the one with strong time-dependent forcing—that is, the time intervals about the CO_2 ramps between [600, 700] and [1050, 1150] yr. It is in these regions where the traditional concept of chaotic attractors does not hold since it is typically based on unstable periodic orbits (Ott 1993) in the phase space, but such orbits cannot exist in the presence of a forcing with a generic time dependence. The only tool that remains for the dynamical characterization of such cases is the snapshot attractor [as discussed, e.g., in Drótos et al. (2015)]. This object is nothing but the set of the endpoints at time t of $N \gg 1$ trajectories initiated in the remote past t_0, earlier than the convergence time t_c to the attractor ($t - t_0 \gg t_c$; in our case $t_c \approx 150$ yr). Moreover, these endpoints define not only the snapshot attractor but also the natural distribution on it. Both the attractor and its distribution move in time. This movement is reflected by the trend of an increase or a decrease in the instantaneous average temperature in the period of the ramps in Fig. 1a. Although we sample the natural distribution with a rather low number ($N = 40$) of realizations, the rather smooth appearance of the graph of the ensemble average suggests that an increase of N would only smooth out even more the temporal fluctuations of this average; the black line can thus be considered to approximate well the expectation value taken with respect to the natural distribution. It should also be mentioned that there is no extra relaxation time needed to reach the snapshot attractor on any point of the CO_2 ramp: at any time instant after t_c we are on the snapshot attractor. We can say that the ensemble reached the snapshot attractor by year 150, but this attractor was yet time independent up to year 600. It started, however, moving after the onset of the CO_2 forcing (year 600), along with its natural distribution, as our ensemble of trajectories traced this out.

To demonstrate that the snapshot attractor is an attracting object at any time instant, we initiate two completely new ensembles at $t_0' = 570$ and $t_0'' = 1020$ years, with the same randomization algorithm as that applied at $t_0 = 0$ [and the CO_2 forcing remains as in Eq. (1)]. The graphs representing the annual mean surface temperatures T averaged over these new ensembles are overlaid in Fig. 1a as a thick red and a thick light orange line, respectively. We see that these lines converge to the original ensemble average (black line), and they reach the latter after $t_c \approx 150$ yr, similar to what we see for the black line after its initialization. As the convergence now takes place during the ramps, when the snapshot attractor depends on time, we conclude that the

[4] In a steady climate like this, "asymptotically long" investigations in time are, in principle, appropriate for characterizing the natural distribution, but it is hard to reach this limit in practice since the convergence takes place only as the power $(-1/2)$ of the length of the time of investigation. For example, even 450 years of steady climate has numerically turned out to be insufficient for reaching the same accuracy as that provided by the 40-member ensemble.

attracting property also holds during climate change periods.[5] Finally, we note that we did not encounter any sign of a potential coexisting other snapshot attractor.

After the onset of the CO_2 ramps up to their end, one can see in Fig. 1a time intervals when the temperature changes approximately linearly. We shall call these intervals temperature ramps.

Plotting the instantaneous standard deviation $\sigma_T(t)$ of the annual mean temperatures of the ensemble as a function of time (Fig. 1b) gives more insight into the nature of the natural distribution. We see from this that the standard deviation remains on the same order of magnitude over the ramp as over the initial plateau.[6] The typical value of $\sigma_T = 0.8$°C is fully consistent with our observation that deviations larger than 2°C are not likely in Fig. 1a since fluctuations beyond 3σ are always rather rare indeed. We emphasize that the standard deviation $\sigma_T(t)$ is a further statistical characteristic of the natural distribution beyond the average and that it is the simplest characteristic of the internal variability on the snapshot attractor of the climate. Figure 1b shows that the internal variability does not change very much over time; it is nevertheless weaker during the upper plateau than during the lower ones. The observation that the standard deviation is larger in colder climates might be associated with the fact that the larger the meridional temperature gradient the more pronounced the baroclinic activity is at midlatitudes.

4. Dynamical hysteresis

To measure the difference between the forcing and the response, an elimination of time and a representation in a variable space appears to be the most appropriate. In Fig. 2 we show the annual mean surface temperature T as a function of the CO_2 concentration c of the same year, for all times (except for the first 200 years, which were dropped in order to eliminate the initial transients before reaching the attractor). We also compare here the three different scales introduced in section 2. Note that a quasi-static response of the system, when the forcing is so slow that the temperature is the same at any time as in a perpetual steady climate with the CO_2 content corresponding to that given time, would lead in such plots to a straight line on the variable plane. As an illustration, we determined the ensemble

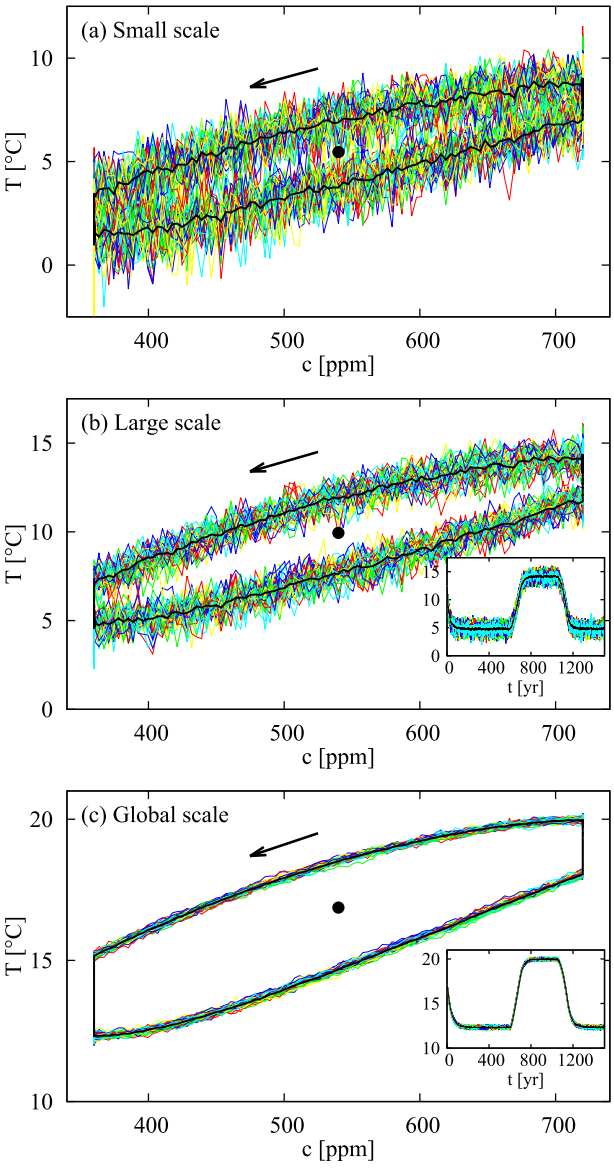

FIG. 2. Hystereses of annual mean surface temperature T as a function of the CO_2 concentration c for the (a) small scale, (b) large scale, and (c) global scale. The insets show these temperatures T as a function of time. [An inset belonging to (a) would coincide with Fig. 1a.] Results for individual ensemble members are plotted in different colors (the same colors as in Fig. 1), and the ensemble average of these values is marked as a black line. The arrows show the direction of the time evolution around the loops. For comparison, we also display the ensemble average of the surface temperature belonging to a perpetual climate with $c = 540$ ppm as single black points. Note the different temperature scales in the different panels. The size of the hysteresis gap is, however, nearly the same in all cases.

[5] The convergence time t_c itself may, in principle, depend on time. Our results, however, indicate that this dependence is weak in our particular model setup (i.e., the strength of the attraction is practically unchanged in time).

[6] In Fig. 1a the spread of the realizations on the temperature ramps appears to be weaker. This is a consequence of the fact that deviation appears in the graphical representation not perpendicularly to the graph of the ensemble average but rather nearly parallel to it. The plotting of the instantaneous standard deviation demonstrates well that an optical illusion is in the background.

average of the surface temperature belonging to a perpetual climate with $c = 540$ ppm and included it in Figs. 2a–c as a single black point.[7] It is clear from Figs. 2a–c that the temperatures belonging to the instantaneous $c = 540$ ppm values in our scenario deviate on both ramps by about 2°C in modulus from that of the perpetual climate on any of the geographical scales investigated.

A large hysteresis loop appears in all cases indicating a nontrivial answer of the system. This is also evident from a comparison of the function of the annual mean temperature $T(t)$ and the function $c(t)$. (This can be best observed in Fig. 1, corresponding to the small scale.) The temperature curves, both as a function of $c(t)$ and of the time t, as demonstrated in Fig. 2, are similar on all scales. The fact that, unlike $c(t)$, they are not piecewise linear is practically equivalent to the existence of the hysteresis loops.

Another remarkable feature here is the dependence on the scale of the observation of the deviation of the individual realizations from the ensemble average. The maximum temperature deviation is on the order of at most 0.5°C on the global scale, and of 1° and 2°C on the large scale and the small scale, respectively. The order of magnitude of the temperature deviations appears to be a strongly decaying function of the number of the grid points taken (see footnote 3). This finding has long been discussed in the literature (see, e.g., Ghil and Mo 1991; Keppenne and Ghil 1993; Goosse et al. 2005). At the same time, the well-developed character of the loop does *not* depend on the scale. Note, however, that the internal variability and the consequent overlap of the graphs is so strong on the small scale that it would not be easy to clearly recognize the hysteresis loop from an individual realization only and that this overlap is also present at the corners of the large-scale plot.

It is worth noting that these three different plots represent three different facets of the evolution of a single snapshot attractor. Determining different geographical means corresponds to finding different projections from the same high-dimensional attractor to a single internal variable (the average temperature corresponding to the particular geographical scale), which is plotted as a function of the forcing. This is why the basic behavior (i.e., the existence of a well-developed loop) is observable on all scales. We note that time series of such projections were found to exhibit low-dimensional dynamics in Fraedrich (1986). We emphasize that the robust existence of the loop implies that it is observable not only in the temperature but in any physical variable (e.g., in the kinetic energy or the enstrophy).

Finally we note that a similar hysteresis (termed memory hysteresis) was found by Bordi et al. (2012) and Fraedrich (2012) in PlaSim in a case when the CO_2 forcing is applied as a periodic decrease (from 360 to 20 ppm) and increase of the concentration, according to a saw-tooth function, at a given rate (1.5 ppm yr^{-1}), without any plateaus. The average surface temperature plotted as a function of the radiative forcing determined from the CO_2 content was shown in these papers to exhibit a hysteresis loop in a single realization.

5. Ensemble averages, single-realization temporal averages, and relaxation times

We now turn to the comparison of the ensemble averages with the averages calculated along single realizations (i.e., along individual members of the ensemble), in the same spirit as in Drótos et al. (2015) treating a low-dimensional model. More precisely, we determine the average in a given time instant t (in fact, we use annual mean values, as explained in section 3) over the ensemble (we shall call it E average), and we also determine the average taken along a single realization over the 30-yr time interval centered on t, called for short the single-realization temporal (SRT) average. The quantity in which we take these averages here is the mean value of the surface temperature, either on the global scale or on the large scale.

To obtain a visual impression on the different character of SRT averages from that of the corresponding E average, we plot in Fig. 3 the E average and the 30-yr SRT averages corresponding to three randomly chosen ensemble members, zoomed in on four time intervals. Each of the four intervals contains a temperature plateau, a part of the approximately linear temperature ramp, and the crossover region between them. One can observe in Figs. 3a–d that the SRT averages fluctuate on the temperature plateaus (i.e., they deviate from the E average). They also exhibit temporal autocorrelation. As a consequence, SRT averages can stay on short temporary plateaus away from the E average (this can be observed easily, e.g., in the green line of Fig. 3c). We also conclude from Fig. 3 that an individual 30-yr SRT average can provide a false impression about climate change; it can show, for example, a warming trend even over several decades when the real expectation value of the temperature does not exhibit any trend (the best example may be the red line of Fig. 3c between years 900 and 950). Although the SRT averages look more smooth during the approximately linear temperature ramps in some cases (see, e.g., Fig. 3b), the fluctuations are still present (even on the global scale; see Fig. 3a). The

[7] The corresponding ensemble standard deviations are on the same order as those in our scenario.

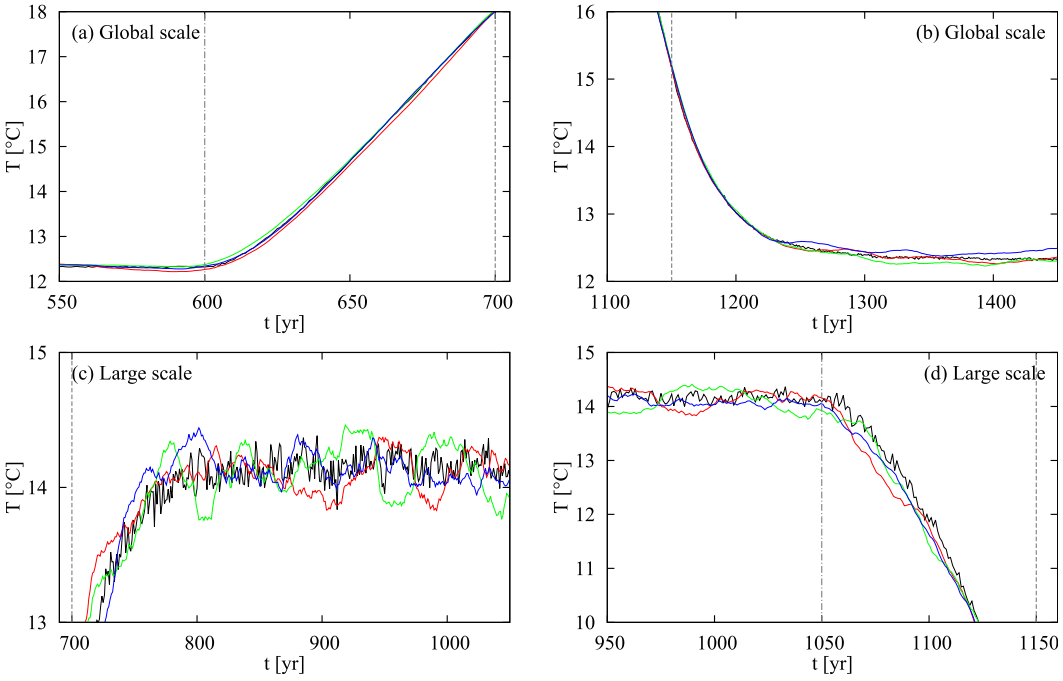

FIG. 3. Annual mean surface temperature T as a function of time. The black line is the E average, and the three colored (red, green, and blue) lines correspond to 30-yr SRT averages taken along three individual ensemble members. The SRT values are plotted at the centers of the 30-yr intervals. The geographical scale is indicated, and two time periods are shown for each of them. The vertical dot–dashed (dashed) line in gray marks the beginning (end) of the CO_2 ramp.

deviation from the E average in the crossover region between the temperature plateau and the approximately linear temperature ramp generally looks stronger than the deviation during the temperature ramp itself (for a good illustration, see Fig. 3d). This observation might stem from the fact that the SRT averages are expected to produce systematic one-sided deviations in the crossover regions since they incorporate the past and the future 15-yr dynamics of the system in any particular time instant. In a steady state (i.e., during the temperature plateaus), however, the natural distribution (of annual means) does not change in time. Furthermore, if this natural distribution were shifted linearly in time, the future and past contributions to the SRT averages would cancel out each other. This is, however, not the case; systematic one-sided deviations are thus expected to occur.

Time intervals of particular interest from a physical point of view are the relaxation intervals to the temperature plateaus (i.e., the time intervals of convergence to the steady climates). We show in Fig. 4 the absolute values of the temperature differences $|\Delta T|$ of the time series from the upper temperature plateau in the relaxation interval to this plateau. (The temperature T_{plat} of the plateau has been calculated by averaging the E average over the time extent $t \in [900, 1050]$ yr of that plateau.) The relaxation is found to be exponential. This is in harmony with the fact that convergence to attractors in dissipative dynamical systems is exponential. Although this statement is well known for constant (or periodic) forcing (Ott 1993), we emphasize that our case is more delicate. The ensemble of our trajectories is on the snapshot attractor in any time instant of the whole relaxation interval. Loosely speaking, we can say that the snapshot attractor itself converges in this time interval toward the usual attractor of a steady climate, corresponding to a hypothetical eternal constant CO_2 plateau. The relaxation time τ of the convergence, defined via $|\Delta T| \sim \exp(-t/\tau)$, is one of the characteristics of the attractor of this hypothetical eternal plateau.

We have numerically calculated the relaxation times τ by fitting lines on the time interval [705, 755] yr to the time series of the logarithms of the above-defined differences $|\Delta T|$. The fitting has been carried out on both the global and the large scale for the E average and for the time series of the individual 30-yr SRT averages, separately for all 40 realizations. For the latter, we have considered their mean and standard deviation. The results are shown in Table 1, in the row labeled "upper plateau." In this table the corresponding results for the small scale are also included, from which we conclude that the characteristics of the relaxation process on the small scale are very similar to those on the large scale.

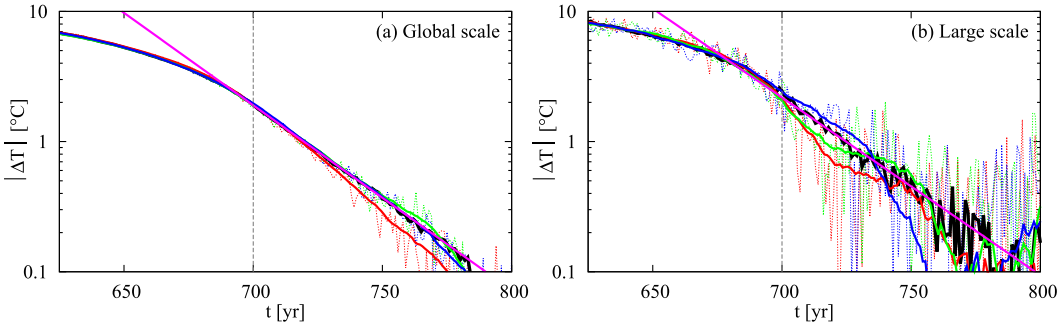

FIG. 4. The temperature difference $|\Delta T|$ from the temperature plateau $T_{plat} = 19.97°C$ (global) and $T_{plat} = 14.16°C$ (large) on a logarithmic scale. The thick black line and the three thick colored lines correspond to the same time series (to the E average and three SRT averages) as in Fig. 3, but the instantaneous temperature difference values of the corresponding realizations are also included as thin colored dashed lines. A linear fit to the black line (on the time interval $t \in [705, 755]$ yr) is also marked by a thick magenta line. The vertical dashed line in gray marks the end of the CO_2 ramp. The geographical scale is indicated.

On the global scale the agreement between the E average time series (black line in Fig. 4a) and the line fitted to this (magenta in Fig. 4a) is very good; the relaxation time of the E average can thus be considered to be precise. The mean value of the individual relaxation times (which happens to be 30.5 yr) is rather close to the value based on the E average. The standard deviation of these individual relaxation times is relatively small. Therefore, we can say that the E average value can roughly be obtained from a typical individual time series of the SRT average in this case. Nevertheless, considerable deviations are also possible between E and SRT averages (see, e.g., the thick red line in Fig. 4b).

As for the large scale, the relaxation time fitted to the E average is reasonably close to the relaxation time obtained on the global scale. What is more, this is still true for the mean value of the individual relaxation times (32.6 yr). The large standard deviation over the ensemble, however, indicates that one particular realization cannot be expected to give a representative value. We emphasize that this fact is not related to the numerical size of the ensemble. Instead, it originates in the spreading of the trajectories on the snapshot attractor according to the well-defined natural distribution on this attractor.

Similar calculations have been carried out for the relaxation to the final plateau with the results shown in Table 1 (row "final plateau"). Practically, the same values (not shown) are obtained for the initial relaxation, in the time interval before year 150. This is in harmony with the fact that the state of the natural distribution on the snapshot attractor in time $t = 1150$ yr can also be considered as an ensemble of initial conditions for the approach to the usual attractor of the hypothetical eternal plateau of $c = 360$ ppm, just as the $t_0 = 0$ ensemble of initial conditions. Note that t_c may be interpreted as approximately 5τ since the approach is practically completed by this time.

The observation that the relaxation times to the final plateau are different from those to the upper plateau (both shown in Table 1) reflects the fact that the two steady climates are of different nature. Note that this is also reflected in the deviation of the hysteresis loops of Fig. 2 from a point-symmetric shape. The large difference between the relaxation times to the final plateau on the global and the large scale is less clear from a theoretical point of view. We have checked that this observation is not sensitive to the particular choice of the time interval used for fitting (which is [1125, 1205] yr for the data shown in Table 1). An

TABLE 1. The fitted relaxation times τ (in years) characterize the approach of the snapshot attractor to the temperature plateaus (i.e., to the steady climates, the usual chaotic attractors). See text for details.

		Global scale	Large scale	Small scale
Upper plateau	τ from E average	30.1	31.8	31.0
	Mean of τ from SRT averages	30.5	32.6	30.2
	Standard deviation of τ from SRT averages	2.9	14.8	13.7
Final plateau	τ from E average	36.3	28.1	28.3
	Mean of τ from SRT averages	35.9	29.4	30.8
	Standard deviation of τ from SRT averages	2.6	9.6	13.9

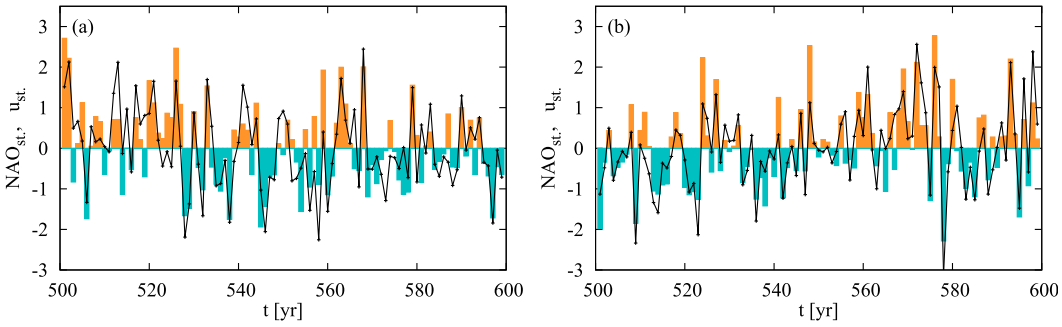

FIG. 5. NAO_{st} (brown and turquoise boxes, depending on the sign) and u_{st} (black crosses connected by a line), determined analogously to NAO_{st}, as a function of time in the time interval [500, 599] yr. (a),(b) Two different realizations are shown.

explanation for this observation needs a more detailed study.

6. Teleconnections

Analyzing long-range relations is of particular interest in the identification of possible teleconnections between different regions of the globe. Such connections—expressed, for example, by indices based on observational data like El Niño–Southern Oscillation (ENSO) or the NAO—are currently intensely studied in meteorology because they may have essential impact on weather patterns even on continental or global scales (Bridgman and Oliver 2006). It is also worth mentioning that many of the various indices used in climate studies are not truly independent of each other (see, e.g., de Viron et al. 2013).

To establish a possible teleconnection analysis in PlaSim climate we now turn to define a simple PlaSim NAO index. This is an extension of the local approach and leads to the difference of two remote gridpoint values.

The NAO is believed to have a significant influence on weather particularly in the North Atlantic region and western Europe, especially via the strength and direction of the westerly winds and storm tracks (Wanner et al. 2001; Hurrell et al. 2003). The NAO is a largely atmospheric mode, and its study is therefore well suited to the standard PlaSim setup with a heat-controlled mixed layer ocean only, used here (see section 2).

There are several possible definitions of the NAO; all have in common that they try to capture fluctuations in the difference of sea level atmospheric pressure between the Azores high and the Icelandic low in a particular season (in what follows, we shall consider the winter season). The most sophisticated definition is based on the principal empirical orthogonal function (EOF) of the pressure field (Barnston and Livezey 1987; Glowienka-Hense 1990). The spirit of a station-based definition, however, seems to better fit for illustrative purposes. In the absence of station-based data, we pick two grid cells in PlaSim: one of them covers Iceland ($\mathcal{I}$), and the other covers the Azores ($\mathcal{A}$).[8] Our NAO index is simply the difference of the sea level pressure $p_{sl,w}$[9] averaged over the winter season [December–February (DJF)] between these two grid cells:

$$\mathrm{NAO}(t) = p_{\mathrm{sl},w,\mathcal{A}}(t) - p_{\mathrm{sl},w,\mathcal{I}}(t), \qquad (2)$$

where time t is measured in years. We also define a standardized index NAO_{st} in steady climates: from a NAO time series [Eq. (2)] of several years, we subtract its time average taken over these years, and then we also divide by the standard deviation taken over this same time interval.

Numerical results for the standardized index NAO_{st}, calculated for the steady climate between years 500 and 599, are shown in Fig. 5 for two particular realizations out of the 40 ensemble members. It is obvious that NAO_{st} exhibits an irregular evolution in time, very similar to that obtained from real observational data (Hurrell and Deser 2010). These time series are also compared to the standardized zonal wind u_{st} determined as the winter mean of the zonal velocity averaged in space over the channel of grid points linking Iceland and the Azores calculated at sigma level 7 (~700 hPa) and standardized afterward. A clear correlation between NAO_{st} and u_{st} can be identified both in Fig. 5a and in Fig. 5b. We thus conclude that our definition for the

[8] The grid indices are as follows: for $\mathcal{I}$, index 60 (i.e., 24°W) in longitude and index 5 (i.e., 64°N) in latitude and for $\mathcal{A}$, index 60 (i.e., 24°W) in longitude and index 10 (i.e., 36°N) in latitude.

[9] The sea level pressure is obtained from PlaSim's surface pressure p_s (which is defined on an average height of 370 m for the grid $\mathcal{I}$, corresponding approximately to a correction of 35 hPa in the pressure) by supposing hydrostatics.

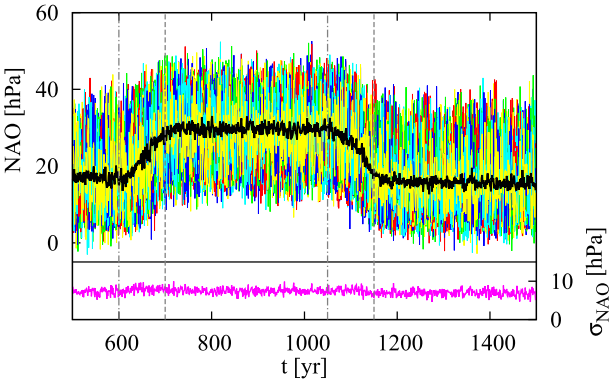

FIG. 6. The nonstandardized NAO index defined by Eq. (2) as a function of time. The individual realizations appear as colored thin lines. The black line is the ensemble average, and the magenta line is the ensemble's standard deviation σ_{NAO}. The vertical dot–dashed (dashed) lines in gray mark the beginning (end) of the CO_2 ramps.

NAO index fairly captures indeed some essential features of the NAO phenomenon.

We emphasize that the particular time series are completely different for the two realizations. In the first 5 years, for example, $\mathrm{NAO}_{\mathrm{st}}$ is of the opposite sign in Fig. 5a versus Fig. 5b. Practically, no common features can be found in the two $\mathrm{NAO}_{\mathrm{st}}$ (or u_{st}) graphs of the figure other than that they both represent random processes. Note that they might be interpreted as two possible time series of measured data in the same climate, one like that of the Earth. In other words, one cannot see from a single realization if it is a "typical" behavior of the climate system. It is also impossible to learn from the observation of the NAO time series on finite time intervals the nature of internal variability (i.e., to figure out what kind of probability distribution the fluctuations obey). We thus conclude again that it is desirable to have an ensemble view.

In this spirit, Fig. 6 shows the NAO index [Eq. (2)] as a function of time (years) for all 40 realizations over the time span between years 500 and 1500 and also its ensemble average and standard deviation. Note that standardization of raw data is meaningful in stationary climates only, and therefore we use nonstandardized values here. The strong fluctuation of any NAO time series is not a surprise in view of the finding of section 4 since the NAO index is a difference of two spatially separated (but correlated) small-scale variables. We see that any single realization fluctuates so much that one can hardly distinguish in them the different behavior on the two plateaus, not to mention the ramps. Typical deviations are on the order of 20 hPa upward (and somewhat smaller downward). It is remarkable that only the ensemble average traces out clearly that there is a considerable difference, of about 60% (on the same order as that of the fluctuations), in the average on the plateaus, connected with a smooth shift over the ramps.[10] These preliminary results already suggest augmenting the usual teleconnection analyses by the snapshot approach in order to avoid the drawbacks of single-realization techniques.

7. Conclusions

The snapshot attractor framework of nonautonomous dynamical systems, like a changing climate system, is advocated as a proper probabilistic view and provides well-defined instantaneous statistical measures (e.g., averages and standard deviations). This approach has been applied so far mainly to low-dimensional examples (Chekroun et al. 2011; Drótos et al. 2015). In this paper our aim was to illustrate the applicability of the basic concepts in the context of an intermediate-complexity climate model rather than making any projections. In particular, we intended to show the following features:

- The snapshot attractor approach is technically feasible in high-degree-of-freedom models, like the Planet Simulator.
- The convergence time for atmospheric phenomena is short (on the order of a century); thus initiation in the very distant past is not needed. Reliable ensemble results can be obtained with reasonable computational resources.
- Typically, individual time series strongly differ from each other in high-degree-of-freedom models.
- Fluctuations in climatic variables increase with decreasing geographical scale; thus, besides the averages, standard deviations (measures of internal variability) become of increasing importance within the snapshot picture.
- A dynamical hysteresis effect exists between the average surface temperature and the CO_2 content, an effect which would be hard to observe based on an individual realization of the dynamics.
- A comparison between the traditional approach of using 30-yr temporal averages and the utilization of ensemble averages leads to significant differences.
- Individual time series of teleconnection measures seem to be noiselike, and they do not provide hints on the current state of the climate system. Only an

[10] The ensemble standard deviation σ_{NAO} (plotted in magenta) is rather insensitive to the CO_2 concentration, which indicates that the internal variability of the NAO stays approximately constant during climate changes and in different "stationary" climates of PlaSim.

ensemble approach can indicate in these measures the sign of a climate change.

These findings rely on the existence of a single snapshot attractor, which characterizes our parameter range. Although there is relevant literature on bifurcations or tipping points in systems with smooth parameter changes (see, e.g., Wieczorek et al. 2011; Ashwin et al. 2012; Nishikawa and Ott 2014), a snapshot analysis is still outstanding. We nevertheless believe that the snapshot framework remains applicable by taking sufficiently localized ensembles to track basins of attractions in such cases.

As for the traditional single snapshot attractor paradigm, it is important to note that one may insist not only to initiate the trajectories at some finite time instant t_0 but also to consider the dynamics (the equations of motion or the forcing) itself to be unknown before this time instant. In this case, one cannot give a meaningful definition for the snapshot attractor before $t_0 + t_c$ (where t_c is the convergence time). The snapshot attractor begins to exist only when the trajectories have forgotten their initial conditions (i.e., at t_c after t_0).

More generally, we argue that the only appropriate probabilistic description of the climate at any instant of time, which fully reflects the internal variability of the dynamics, is the natural distribution of the snapshot attractor corresponding to this time instant, applicable in practice even to GCMs. Thus the proper approach to characterize any climate change is to follow the temporal evolution of this distribution in time. An important consequence of the latter observation is that the individual 30-yr (or any multidecadal) averages might be misleading.

Acknowledgments. Valuable discussions with E. Kirk and F. Lunkeit are gratefully acknowledged. Thanks are due to them and to all members of the Theoretical Meteorology group at Meteorological Institute, University of Hamburg, for introducing us into the world of PlaSim. We benefited from useful comments by T. Bódai, T. Haszpra, I. M. Jánosi, Z. Rácz, M. Vincze, and T. Weidinger. T. T. is grateful for support from the Alexander von Humboldt Foundation. This work was also supported by the Hungarian Science Foundation under Grant NK100296. We are thankful for the useful remarks of an anonymous referee and of M. Ghil and K. Fraedrich, who identified themselves as the second and the third referees.

REFERENCES

Arnold, L., 1998: *Random Dynamical Systems.* Springer, 586 pp.

Ashwin, P., S. Wieczorek, R. Vitolo, and P. Cox, 2012: Tipping points in open systems: Bifurcation, noise-induced and rate-dependent examples in the climate system. *Philos. Trans. Roy. Soc. London*, **370A**, 1166–1184, doi:10.1098/rsta.2011.0306.

Barnston, A. G., and R. E. Livezey, 1987: Classification, seasonality and persistence of low-frequency atmospheric circulation patterns. *Mon. Wea. Rev.*, **115**, 1083–1126, doi:10.1175/1520-0493(1987)115<1083:CSAPOL>2.0.CO;2.

Bódai, T., and T. Tél, 2012: Annual variability in a conceptual climate model: Snapshot attractors, hysteresis in extreme events, and climate sensitivity. *Chaos*, **22**, 023110, doi:10.1063/1.3697984.

——, G. Károlyi, and T. Tél, 2011: Fractal snapshot components in chaos induced by strong noise. *Phys. Rev.*, **83E**, 046201, doi:10.1103/PhysRevE.83.046201.

Bordi, I., K. Fraedrich, A. Sutera, and X. Zhu, 2012: Transient response to well-mixed greenhouse gas changes. *Theor. Appl. Climatol.*, **109**, 245–252, doi:10.1007/s00704-011-0580-z.

Bridgman, H. A., and J. E. Oliver, 2006: *The Global Climate System: Patterns, Processes, and Teleconnections.* Cambridge University Press, 358 pp.

Bye, J., K. Fraedrich, E. Kirk, S. Schubert, and X. Zhu, 2011: Random walk lengths of about 30 years in global climate. *Geophys. Res. Lett.*, **38**, L05806, doi:10.1029/2010GL046333.

Carvalho, A. N., J. A. Langa, and J. C. Robinson, 2013: *Attractors for Infinite-Dimensional Non-autonomous Dynamical Systems.* Applied Mathematical Sciences, Vol. 182, Springer, 412 pp.

Chekroun, M. D., E. Simonnet, and M. Ghil, 2011: Stochastic climate dynamics: Random attractors and time-dependent invariant measures. *Physica D*, **240**, 1685–1700, doi:10.1016/j.physd.2011.06.005.

Daron, J. D., and D. A. Stainforth, 2013: On predicting climate under climate change. *Environ. Res. Lett.*, **8**, 034021, doi:10.1088/1748-9326/8/3/034021.

——, and ——, 2015: On quantifying the climate of the non-autonomous Lorenz-63 model. *Chaos*, **25**, 043103, doi:10.1063/1.4916789.

Deser, C., R. Knutti, S. Solomon, and A. S. Phillips, 2012a: Communication of the role of natural variability in future North American climate. *Nat. Climate Change*, **2**, 775–779, doi:10.1038/nclimate1562.

——, A. Phillips, V. Bourdette, and H. Teng, 2012b: Uncertainty in climate change projections: The role of internal variability. *Climate Dyn.*, **38**, 527–546, doi:10.1007/s00382-010-0977-x.

de Viron, O., J. O. Dickey, and M. Ghil, 2013: Global modes of climate variability. *Geophys. Res. Lett.*, **40**, 1832–1837, doi:10.1002/grl.50386.

Dijkstra, H. A., and M. Ghil, 2005: Low-frequency variability of the large-scale ocean circulation: A dynamical systems approach. *Rev. Geophys.*, **43**, RG3002, doi:10.1029/2002RG000122.

Drótos, G., T. Bódai, and T. Tél, 2015: Probabilistic concepts in a changing climate: A snapshot attractor picture. *J. Climate*, **28**, 3275–3288, doi:10.1175/JCLI-D-14-00459.1.

Feliks, Y., and M. Ghil, 2011: The atmospheric circulation over the North Atlantic as induced by the SST field. *J. Climate*, **24**, 522–542, doi:10.1175/2010JCLI3859.1.

Fraedrich, K., 1986: Estimating the dimensions of weather and climate attractors. *J. Atmos. Sci.*, **43**, 419–432, doi:10.1175/1520-0469(1986)043<0419:ETDOWA>2.0.CO;2.

——, 2012: A suite of user-friendly global climate models. Hysteresis experiments. *Eur. Phys. J. Plus*, **127**, doi:10.1140/epjp/i2012-12053-7.

——, and F. Lunkeit, 2008: Diagnosing the entropy budget of a climate model. *Tellus*, **60A**, 921–931, doi:10.1111/j.1600-0870.2008.00338.x.

——, E. Kirk, and F. Lunkeit, 1998: PUMA: Portable university model of the atmosphere. Deutsches Klimarechenzentrum Tech. Rep. 16, 37 pp.

——, H. Jansen, E. Kirk, U. Luksch, and F. Lunkeit, 2005a: The Planet Simulator: Towards a user friendly model. *Meteor. Z.*, **14**, 299–304, doi:10.1127/0941-2948/2005/0043.

——, E. Kirk, U. Luksch, and F. Lunkeit, 2005b: The portable university model of the atmosphere (PUMA): Storm track dynamics and low-frequency variability. *Meteor. Z.*, **14**, 735–745, doi:10.1127/0941-2948/2005/0074.

Ghil, M., 2012: The complex physics of climate change and climate sensitivity: A grand unification (Alfred Wegener Medal Lecture). *European Geosciences Union General Assembly 2012*, Vienna, Austria, European Geosciences Union, EGU2012-14438-1.

——, and K. Mo, 1991: Intraseasonal oscillations in the global atmosphere. Part I: Northern Hemisphere and tropics. *J. Atmos. Sci.*, **48**, 752–779, doi:10.1175/1520-0469(1991)048<0752:IOITGA>2.0.CO;2.

——, M. D. Chekroun, and E. Simonnet, 2008: Climate dynamics and fluid mechanics: Natural variability and related uncertainties. *Physica D*, **237**, 2111–2126, doi:10.1016/j.physd.2008.03.036.

Glowienka-Hense, R., 1990: The North Atlantic Oscillation in the Atlantic-European SLP. *Tellus*, **42A**, 497–507, doi:10.1034/j.1600-0870.1990.t01-3-00001.x.

Goosse, H., H. Renssen, A. Timmermann, and R. S. Bradley, 2005: Internal and forced climate variability during the last millennium: a model-data comparison using ensemble simulations. *Quat. Sci. Rev.*, **24**, 1345–1360, doi:10.1016/j.quascirev.2004.12.009.

Hasselmann, K., 1976: Stochastic climate models: Part 1. Theory. *Tellus*, **28A**, 473–485, doi:10.1111/j.2153-3490.1976.tb00696.x.

Hurrell, J. W., and C. Deser, 2010: North Atlantic climate variability: The role of the North Atlantic Oscillation. *J. Mar. Syst.*, **79**, 231–244, doi:10.1016/j.jmarsys.2009.11.002.

——, Y. Kushnir, G. Ottersen, and M. Visbeck, 2003: *The North Atlantic Oscillation: Climatic Significance and Environmental Impact. Geophys. Monogr.*, Vol. 134, Amer. Geophys. Union, 279 pp.

IPCC, 2013: *Climate Change 2013: The Physical Science Basis*. Cambridge University Press, 1535 pp.

Keppenne, C. L., and M. Ghil, 1993: Adaptive filtering and prediction of noisy multivariate signals: An application to subannual variability in atmospheric angular momentum. *Int. J. Bifurcat. Chaos*, **3**, 625–634, doi:10.1142/S0218127493000520.

Kloeden, P., and M. Rasmussen, 2011: *Nonautonomous Dynamical Systems.* American Mathematical Society, 264 pp.

Lacis, A. A., and J. E. Hansen, 1974: A parameterization for the absorption of solar radiation in the earth's atmosphere. *J. Atmos. Sci.*, **31**, 118–133, doi:10.1175/1520-0469(1974)031<0118:APFTAO>2.0.CO;2.

Lucarini, V., K. Fraedrich, and F. Lunkeit, 2010: Thermodynamic analysis of snowball earth hysteresis experiment: Efficiency, entropy production, and irreversibility. *Quart. J. Roy. Meteor. Soc.*, **136**, 2–11, doi:10.1002/qj.543.

Lunkeit, F., and Coauthors, 2011: Planet Simulator reference manual version 16. Meteorological Institute Rep., 85 pp.

Nishikawa, T., and E. Ott, 2014: Controlling systems that drift through a tipping point. *Chaos*, **24**, 033107, doi:10.1063/1.4887275.

Orszag, S. A., 1970: Transform method for calculation of vector-coupled sums: Application to the spectral form of the vorticity equation. *J. Atmos. Sci.*, **27**, 890–895, doi:10.1175/1520-0469(1970)027<0890:TMFTCO>2.0.CO;2.

Ott, E., 1993: *Chaos in Dynamical Systems.* Cambridge University Press, 492 pp.

Paillard, D., 2008: From atmosphere, to climate, to Earth system science. *Interdiscip. Sci. Rev.*, **33**, 25–35, doi:10.1179/030801808X259943.

Pierrehumbert, R. T., 2010: *Principles of Planetary Climate*. Cambridge University Press, 674 pp.

Ragone, F., V. Lucarini, and F. Lunkeit, 2015: A new framework for climate sensitivity and prediction: A modelling perspective. *Climate Dyn.*, doi:10.1007/s00382-015-2657-3, in press.

Romeiras, F. J., C. Grebogi, and E. Ott, 1990: Multifractal properties of snapshot attractors of random maps. *Phys. Rev.*, **41A**, 784, doi:10.1103/PhysRevA.41.784.

Roscher, M., F. Stordal, and H. Svenson, 2011: The effect of global warming and global cooling on the distribution of the latest Permian climate zones. *Palaeogeogr. Palaeoclimatol. Palaeoecol.*, **309**, 186–200, doi:10.1016/j.palaeo.2011.05.042.

Sasamori, T., 1968: The radiative cooling calculation for application to general circulation experiments. *J. Appl. Meteor.*, **7**, 721–729, doi:10.1175/1520-0450(1968)007<0721:TRCCFA>2.0.CO;2.

Stainforth, D. A., and Coauthors, 2005: Uncertainty in predictions of the climate response to rising levels of greenhouse gases. *Nature*, **433**, 403–406, doi:10.1038/nature03301.

Stephens, G. L., S. Ackerman, and E. A. Smith, 1984: A shortwave parameterization revised to improve cloud absorption. *J. Atmos. Sci.*, **41**, 687–690, doi:10.1175/1520-0469(1984)041<0687:ASPRTI>2.0.CO;2.

Stephens, M. Y., R. J. Oglesby, and M. Maxey, 2005: A one-dimensional mixed layer ocean model for use in three-dimensional climate simulations: Control simulation compared to observations. *J. Climate*, **18**, 2199–2221, doi:10.1175/JCLI3380.1.

Wanner, H., S. Brönnimann, C. Casty, D. Gyalistras, J. Luterbacher, C. Schmutz, D. B. Stephenson, and E. Xoplaki, 2001: North Atlantic Oscillation—Concepts and studies. *Surv. Geophys.*, **22**, 321–382, doi:10.1023/A:1014217317898.

Washington, W. M., and C. L. Parkinson, 2005: *An Introduction to Three-Dimensional Climate Modeling.* University Science Books, 354 pp.

Wieczorek, S., P. Ashwin, C. M. Luke, and P. M. Cox, 2011: Excitability in ramped systems: The compost-bomb instability. *Proc. Roy. Soc. London*, **467A**, 1243–1269, doi:10.1098/rspa.2010.0485.